

SN 1986J VLBI. II. THE EVOLUTION OF THE SHELL AND THE CENTRAL SOURCE

M. F. BIETENHOLZ^{1,2}, N. BARTEL² AND M. P. RUPEN³

Version 8.1 November 17, 2018

ABSTRACT

We present new VLBI images of supernova 1986J, taken at 5, 8.4 and 22 GHz between $t = 22$ to 25 yr after the explosion. The shell expands $\propto t^{0.69 \pm 0.03}$. We estimate the progenitor's mass-loss rate at $(4 \sim 10) \times 10^{-5} M_{\odot} \text{ yr}^{-1}$ (for $v_w = 10 \text{ km s}^{-1}$). Two bright spots are seen in the images. The first, in the northeast, is now fading. The second, very near the center of the projected shell and unique to SN 1986J, is still brightening relative to the shell, and now dominates the VLBI images. It is marginally resolved at 22 GHz (diameter $\sim 0.3 \text{ mas}$; $\sim 5 \times 10^{16} \text{ cm}$ at 10 Mpc). The integrated VLA spectrum of SN 1986J shows an inversion point and a high-frequency turnover, both progressing downward in frequency and due to the central bright spot. The optically-thin spectral index of the central bright spot is indistinguishable from that of the shell. The small proper motion of $1500 \pm 1500 \text{ km s}^{-1}$ of the central bright spot is consistent with our previous interpretation of it as being associated with the expected black-hole or neutron-star remnant. Now, an alternate scenario seems also plausible, where the central bright spot, like the northeast one, results when the shock front impacts on a condensation within the circumstellar medium (CSM). The condensation would have to be so dense as to be opaque at cm wavelengths ($\sim 10^3 \times$ denser than the average corresponding CSM) and fortuitously close to the center of the projected shell. We include a movie of the evolution of SN 1986J at 5 GHz from $t = 0$ to 25 yr.

Subject headings: supernovae: individual (SN 1986J) — radio continuum: supernovae

1. INTRODUCTION

Supernova 1986J was one of the most radio luminous supernovae ever observed. Its long-lasting and strong radio emission and its relative nearness makes it one of the few supernovae for which it is possible to produce detailed images with very-long-baseline interferometry (VLBI), in addition to being one of the few supernovae still detectable more than $t = 20$ years after the explosion.

SN 1986J was first discovered in the radio, some time after the explosion (van Gorkom et al. 1986; Rupen et al. 1987). The best estimate of the explosion epoch is 1983.2 ± 1.1 ($t = 0$, Bietenholz et al. 2002, see also Rupen et al. 1987; Chevalier 1987; Weiler et al. 1990). It occurred in the nearby galaxy NGC 891, whose distance is $\sim 10 \text{ Mpc}$ (see e.g., Tonry et al. 2001; Ferrarese et al. 2000; Tully 1988; Kraan-Korteweg 1986; Aaronson et al. 1982). We will adopt the round value of 10 Mpc throughout this paper.

Early optical spectra showed that the supernova was unusual, but based on its prominent H α lines it was classified as a Type II_n supernova (Rupen et al. 1987). Later, Leibundgut et al. (1991) suggested that it might be of Type Ib. VLBI observations started soon after discovery (Bartel et al. 1987), and an image, the first of any optically identified supernova, was obtained soon after (Bartel et al. 1991), and showed a heavily modulated shell structure with protrusions. VLBI observations at subsequent epochs up to 1999 led to a series of

images showing the expansion of the shell, and allowing the expansion velocity and deceleration to be measured (Bietenholz et al. 2002).

The evolution of the radio spectrum of a supernova is in most cases predictable. In particular, once supernovae have become optically thin after a few months or years, they usually display power-law radio spectra with spectral indices, α , in the range of -0.8 to -0.5 ($S \propto \nu^{\alpha}$). SN 1986J also showed such a spectrum before 1998, but a remarkable change occurred after that. An inversion appeared in the spectrum, with the brightness increasing with increasing frequency above $\sim 10 \text{ GHz}$, and a high-frequency turnover at $\sim 20 \text{ GHz}$ (Bietenholz et al. 2002).

This spectral inversion was associated with a bright spot in the (projected) center of the expanding shell, as we showed in Bietenholz et al. (2004a) using phase-referenced multi-frequency VLBI imaging. At that time (late 2002) the bright spot was clearly present in the 15 GHz image, but not discernible in the 5 GHz one. We report here on new VLBI and VLA observations of SN 1986J which show the further evolution of this unique object.

2. OBSERVATIONS AND DATA REDUCTION

2.1. VLBI Measurements

The VLBI observations of SN 1986J were made between 2005 and 2008 with global VLBI arrays of 13 to 18 antennas and with durations of 12 to 15 hours. The observations of SN 1986J were interleaved with ones of 3C 66A, only $40'$ away on the sky, which we used as a phase-reference source. Details of the four observing runs are given in Table 1. The declination of $+42^{\circ}$ of SN 1986J enabled us to obtain dense and only moderately elliptical u - v coverage. As usual, a hydrogen maser was used as a time and frequency standard at each telescope. The data

¹ Hartebeesthoek Radio Observatory, PO Box 443, Krugersdorp, 1740, South Africa

² Department of Physics and Astronomy, York University, Toronto, M3J 1P3, Ontario, Canada

³ National Radio Astronomy Observatory, Socorro, New Mexico 87801, USA

Table 1
VLBI Observations of SN 1986J

Date	Frequency (GHz)	Antennas ^a	Total time (hr)	Recording rate (Mbits s ⁻¹)
2005 Apr 25	22	VLBA, Ef, Gb, Y27	12	256
2005 Oct 24	5	VLBA, Ef, Gb, Y27, Jb, On, Wb, Tr	12	256
2006 Dec 3	8	VLBA, Ef, Gb, Y27	15	512
2006 Dec 10	22	VLBA, Ef, Gb, Y27	15	512
2008 Oct 26	5	VLBA, Ef, GB, Y27, Jb, Mc, Nt, Tr, Wb	18	512

^a VLBA, ten 25 m dishes of the NRAO Very Long Baseline Array; Ef, 100 m, MPIFR, Effelsberg, Germany; Gb, 105 m, NRAO, Green Bank, WV, USA; Y27, equivalent diameter 130 m, NRAO, near Socorro, NM, USA; Jb, 76 m, Jodrell Bank, UK; Mc, 32 m, IdR-CNR, Medicina, Italy; Nt, 32 m, IdR-CNR, Noto, Italy; On, 20 m, Onsala Space Observatory, Sweden; Tr, 32 m, Torun, Poland; Wb, equivalent diameter 94 m, Westerbork, the Netherlands.

were recorded with either the VLBA or the MKIV VLBI system with sampling rates of 256 or 512 Mbits per second. We observed at frequencies of 5.0, 8.4 and 22 GHz. The data were correlated with the NRAO⁴ VLBA processor in Socorro, NM (USA), and the analysis was carried out with NRAO’s Astronomical Image Processing System (AIPS). The initial flux density calibration was done through measurements of the system temperature at each telescope, and improved through self-calibration of the 3C 66A data.

We phase-referenced to 3C 66A for all of the present observing runs. Our positions in this paper are given relative to an assumed position of RA = 02^h 22^m 39^s.611500, decl. = 43° 02′ 07[″].79884 taken from the International Celestial Reference Frame, ICRF (Fey et al. 2004). for the brightness peak of 3C 66A.

2.2. VLA Observations

In addition to the VLBI observation, we also obtained VLA observations to measure SN 1986J’s total flux density at a range of different frequencies, both during our VLBI observations and at other times. We also reduced a number of data sets from the VLA archives in order to obtain additional flux density measurements. The epochs and the frequencies observed are listed in Table 2. These observations allowed us to monitor the evolution of SN 1986J’s integrated radio spectrum.

The VLA data were reduced following standard procedures, with the flux density scale calibrated by using observations of the standard flux density calibrators (3C 286 and 3C 48) on the scale of Baars et al. (1977). An atmospheric opacity correction using mean zenith opacities was applied, and NGC 891/SN 1986J was self-calibrated in phase to the extent permitted by the signal-to-noise ratio for each epoch and frequency. At lower resolutions the supernova cannot be reliably separated from the diffuse emission from the galaxy. Therefore, we cite only flux densities obtained at FWHM resolutions⁵ of < 7[″]. For the 0.33 GHz measurements we incorporate an additional uncertainty to reflect the difficulty of accurate galaxy subtraction.

We note also that the gradual introduction of EVLA

antennas into the VLA array might cause some problems in the flux-density calibration. Since the bandpass of the EVLA antennas differs from that of the older VLA-antennas, non-closing offsets are introduced for continuum observations such as ours, with the gain of an EVLA-EVLA baseline being typically several percent higher than that of a VLA-VLA baseline. Such non-closing offsets cannot be calibrated out using only standard procedures, which assume that the gains are dependent only on the antennas, and not on the baseline. These closure errors might compromise the accuracy of the flux density calibration. To determine whether this effect is significant, we carried out, for several epochs and frequencies, a more elaborate flux-density calibration scheme using baseline-dependent factors calculated by the AIPS task BLCAL. Although the more elaborate calibration led to an improvement in the dynamic range, in no case was the normal flux-density scale in error by more than 1%. Since we include in all cases a flux-density calibration uncertainty of ≥ 5%, we can say that any errors introduced by the use of the EVLA antennas are well within our stated uncertainties.

In Table 2 we list the total flux density measurements that we obtained from VLA observations. Note that some of these values have been previously published (see Bietenholz & Bartel 2008a; Bietenholz et al. 2005, 2004a), but we repeat them here for the convenience of the reader and to allow a better interpretation of the evolution of SN 1986J’s radio emission.

We plot a selection of these flux densities in two ways: first, in Figure 1, we plot the evolution of the flux-density as a function of time at several different frequencies. Second, in Figure 2 we plot the radio spectrum as a function of time at a number of epochs. We focus in this paper on the flux-density evolution in the last decade, for lightcurves covering the earlier part of SN 1986J’s evolution, see Bietenholz et al. (2002) and Weiler et al. (1990).

Figure 1 shows that the flux density at all our observing frequencies is generally decreasing. In terms of a power-law decay with $S_\nu \propto t^\beta$, a weighted least-squares fit gives an average value of $\beta = -2.2$ over the last decade and over the frequencies of 1.5, 5.0, 8.4, 15 and 22 GHz, with the fastest decay seen at 1.5 GHz with $\beta = -3.3$ and the slowest at 15 GHz with $\beta = -1.0$.

⁴ The National Radio Astronomy Observatory, NRAO, is a facility of the National Science Foundation operated under cooperative agreement by Associated Universities, Inc.

⁵ We take the geometric mean of the major and minor axes of the elliptical Gaussian fit to the dirty beam as our measure of resolution.

Table 2
Flux Densities of SN 1986J from VLA Observations

Date	Flux densities ^a						
	0.32 GHz	1.43 GHz	4.9 GHz ^b	8.4 GHz ^c	14.9 GHz	22 GHz ^d	43.3 GHz
1995 Jun 22 ^e		25.6 ± 1.3	14.2 ± 0.8		9.1 ± 0.7	8.0 ± 0.8	
1996 Oct 25 ^e			11.0 ± 0.6	8.7 ± 0.5			
1997 Jan 31 ^e				8.2 ± 0.5			
1998 Feb 9 ^e					5.65 ± 0.69	9.3 ± 1.5	
1998 Jun 5		13.7 ± 0.9 ^f	8.5 ± 0.5	7.2 ± 0.4			
1999 Feb 2			7.3 ± 1.5	6.1 ± 0.4	6.1 ± 0.1	9.5 ± 1.0	
1999 Jun 13 ^e		11.69 ± 0.62		5.68 ± 0.30	4.92 ± 0.52		
2000 Oct 19 ^e		8.97 ± 0.47	5.43 ± 0.29	4.76 ± 0.26	5.88 ± 0.42	5.67 ± 0.65	
2001 Jan 25 ^e		9.02 ± 0.22		4.75 ± 0.36			
2002 Jan 27 ^e		7.68 ± 0.46	4.15 ± 0.26	4.13 ± 0.28	5.02 ± 0.54	4.22 ± 0.44	
2002 May 25		7.10 ± 0.70	4.20 ± 0.30	3.80 ± 0.30	4.70 ± 0.50	5.00 ± 0.60	3.9 ^{+2.1} _{-0.9}
2002 Nov 11			3.86 ± 0.28	4.16 ± 0.25		5.37 ± 0.50	
2003 Jan 8			3.75 ± 0.45	3.75 ± 0.30	4.25 ± 0.44	4.41 ± 0.48	3.90 ± 0.50
2003 Jun 22		6.63 ± 0.57	3.50 ± 0.25	3.88 ± 0.20	4.57 ± 0.70		
2004 Jan 31 ^e					4.72 ± 0.29	4.74 ± 0.27	
2004 Sep 23		4.55 ± 0.33	3.07 ± 0.20	3.45 ± 0.20	4.44 ± 0.26	4.79 ± 0.49	3.59 ± 0.40
2005 Jan 8		4.49 ± 0.33	2.91 ± 0.16	3.21 ± 0.19	4.01 ± 0.27	4.11 ± 0.23	3.18 ± 0.38
2005 Apr 26			2.58 ± 0.43	2.92 ± 0.17	3.14 ± 1.12	3.73 ± 0.28	
2005 Jun 13 ^e			2.45 ± 0.17	3.11 ± 0.19	4.01 ± 0.34	3.75 ± 0.59	
2005 Oct 10						4.25 ± 0.55	
2006 Mar 6		3.99 ± 0.26	2.62 ± 0.17	3.20 ± 0.16	3.92 ± 0.26	3.93 ± 0.20	2.91 ± 0.35
2006 Jun 6			2.45 ± 0.15	3.20 ± 0.17	4.16 ± 0.35	3.61 ± 0.21	2.32 ± 0.34
2006 Aug 30 ^e			2.12 ± 0.13			3.24 ± 0.43	
2006 Dec 4				3.13 ± 0.31			
2006 Dec 11						4.54 ± 0.91	
2007 Apr 23					3.69 ± 0.29	3.57 ± 0.20	2.07 ± 0.29
2007 Jul 31			2.06 ± 0.15		3.77 ± 0.32		
2007 Aug 19 ^g	8.9 ± 1.8	3.07 ± 0.13		2.97 ± 0.12			
2007 Aug 23 ^h						3.12 ± 0.19	2.13 ± 0.23
2008 Oct 26			2.27 ± 0.12				

^a Flux densities from fitting images and/or fitting $u-v$ plane models. The tabulated uncertainties include a systematic uncertainty in the flux density calibration of 5% or more at frequencies of 22 GHz and below, and 10% or more at 43 GHz. They also include the estimated uncertainty of the galaxy subtraction for those epochs/frequencies at which the galaxy contribution was significant. We only tabulate measurements at resolutions $< 7''$, and ones where the galaxy contribution was $< 50\%$ of the brightness of SN 1986J.

^b Observations between 4.86 and 4.99 GHz.

^c Observations between 8.41 and 8.46 GHz.

^d Observations between 22.21 and 22.66 GHz.

^e Data from the VLA archives.

^f Flux density at 1.7 GHz, rather than 1.43 GHz.

^g Values are the average from two observing runs on 2007 Jul 31 and 2007 Sep 6.

^h Values are the average from two observing runs on 2007 Jul 31 and 2007 Sep 15.

2.3. Radio Spectral Index

As is clear from Figure 2, the radio spectral index, α is a strong function of both time and frequency. Up to 1995.5, however, the spectrum at least between 1.4 and 15 GHz seems well described by a single power-law. Earlier on, up to 1988, Weiler et al. (1990) reported a spectral index for the optically-thin part of $-0.67^{+0.08}_{-0.04}$. Ball & Kirk (1995), for the period up to 1991, find a somewhat flatter value of -0.57 ± 0.01 from fitting a diffusive acceleration model. Fitting a power-law to the first set of flux densities included in Table 1, namely those of 1995.5, we find a notably flatter spectrum, with a spectral index of -0.44 ± 0.03 (we note that if we drop the 22 GHz flux density from this fit on the suspicion that it might already be contaminated by the inversion, the fitted spectral index changes by less than the uncertainties). So the spectrum seems to have flattened significantly between 1988 and 1995.

After 1995, the inversion appears in the spectrum, and its evolution becomes more complex. We will focus first

on the low-frequency part of the spectrum, which we associate with the shell. In Bietenholz et al. (2002), we performed a two-part decomposition of the spectrum for the period 1998 to 2002, and obtained a spectral index of $-0.55^{+0.09}_{-0.16}$. For even more recent times, we can calculate some representative spectral indices from the flux densities in Table 1. From our measurements on 2007 Aug 19, we find $\alpha_{0.3\text{GHz}}^{1.4\text{GHz}} = -0.71 \pm 0.14$. Although the uncertainties are rather large, this suggests also that the part of the spectrum at the lowest frequencies is again becoming steeper since 1995.5.

In summary, the evidence suggests that the part of the spectrum below the inversion, which we associate with the shell, was fairly steep with $\alpha \simeq -0.62$ at times till 1988, flattening to $\alpha \simeq -0.44$ in 1995, and once again steepening somewhat to $\alpha \simeq -0.7$ since then. By averaging the spectral indices derived by us and others for the low-frequency/optically-thin part of the spectrum, we find an average value over the whole timerange of -0.61 with an rms of 0.11.

Another region of interest is the spectrum *above* the high-frequency turnover. This part of the spectrum is

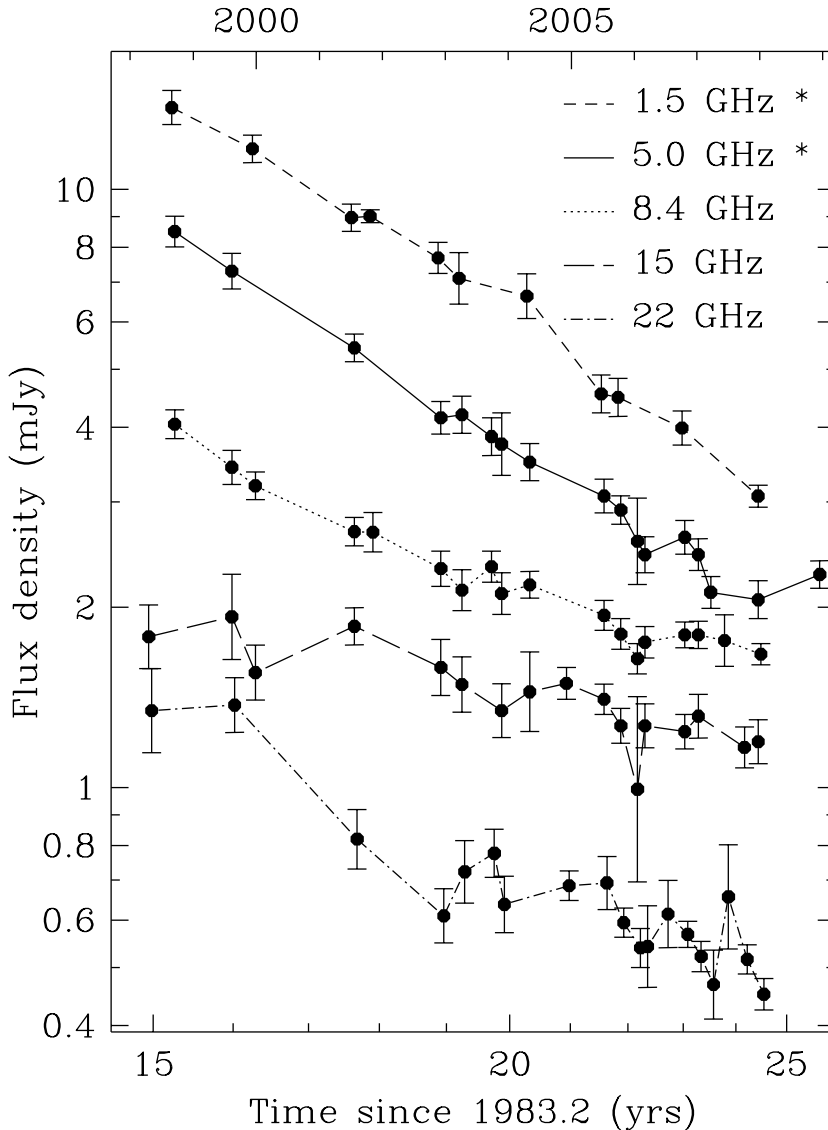


Figure 1. Multi-frequency radio lightcurves for SN 1986J, as determined from VLA observations. We plot the lightcurves at 1.4, 5.0, 8.4, 15, and 22 GHz. The flux-density scale on the left axis is relevant directly for the lightcurves at 1.5 and 5.0 GHz (marked with an asterisk), while those at 8.4, 15 and 22 GHz are shifted logarithmically downwards for better visibility, so that the shape of the lightcurve is preserved even though the flux density scale is not. The curves are shifted by the following factors: 8.4 GHz by 0.56, 15 GHz by 0.32, and 22 GHz by 0.14. The uncertainties are estimated standard errors, including statistical and systematic contributions. The data include both our own and re-reduced archival data (see Table 2).

dominated by emission from the central bright spot, and thus presumably represents its unabsorbed spectrum. A weighted average between 2006 Mar 6 and 2007 Aug 23 gives $\alpha_{22\text{GHz}}^{44\text{GHz}} = -0.61 \pm 0.11$.

3. VLBI IMAGES

In Figures 3 and 4 we show the VLBI images of SN 1986J at the different frequencies and dates in Table 1. For comparison, we include in Figure 3 also some of our previously published images from 1999 and 2002. We discuss the images in turn, first those at 5 GHz, which together with the earlier images present the best picture of the evolution of the supernova, and then those at 8.4 and 22 GHz.

Since all the observations in this paper were phase-

referenced to the brightness peak of 3C 66A, which is expected to be closely related to the core of the galaxy, we can accurately align the images of SN 1986J at different times and frequencies to facilitate inter-comparison. Unfortunately, since the earliest epochs of VLBI observations of SN 1986J (between 1987 and 1992, see Bietenholz et al. 2002) were not phase-referenced, we cannot pinpoint the explosion location accurately, as we did for SN 1993J (see Bietenholz et al. 2001). However, we can visually estimate the position of the center of the shell sufficiently accurately for our purposes. We use this center position as the origin of our coordinate system in all the images, and also as our estimate of the explosion location.

In particular, we estimated by eye the coordinates

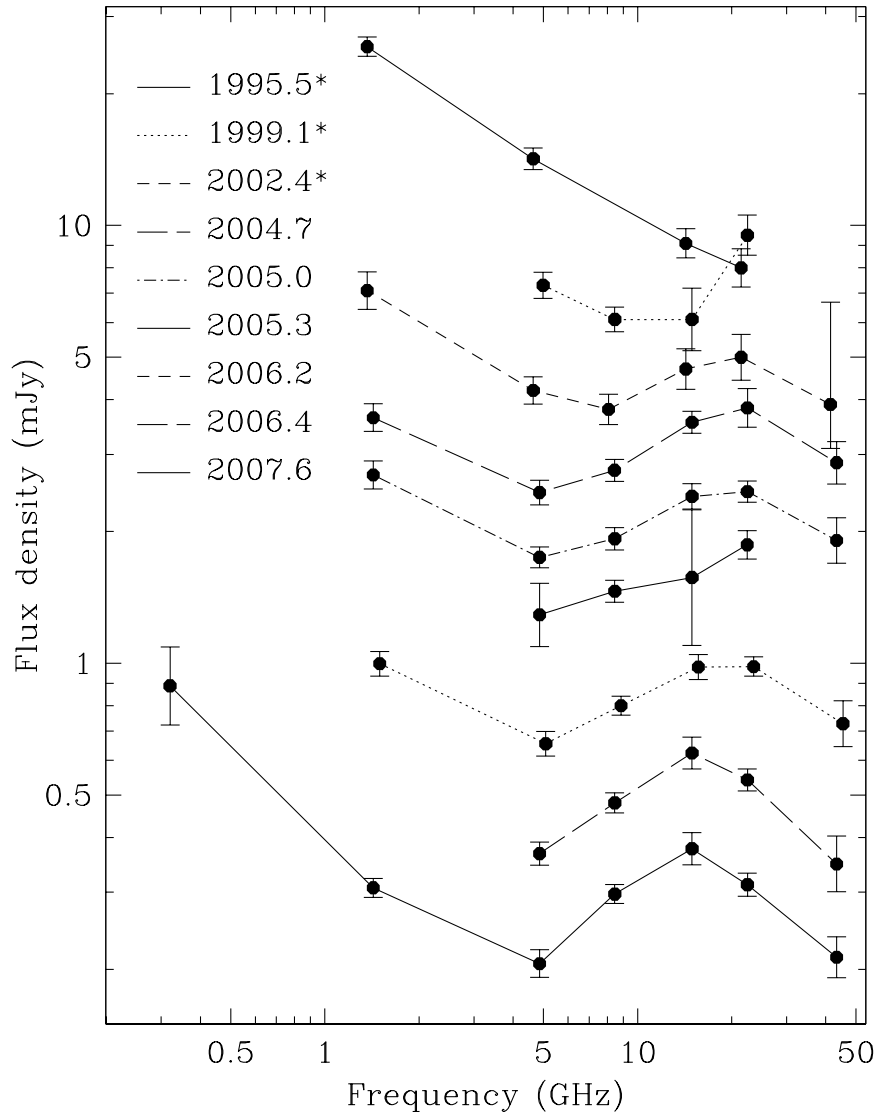


Figure 2. The evolving radio spectrum of SN 1986J, as determined from VLA observations. Each curve shows the radio spectrum at the epoch indicated at left, with the earliest spectrum at the top. The flux-density scale on the left axis is relevant directly for the first three curves from the top (1995.5, 1999.1 and 2002.4), whose epochs are marked with an asterisk. The other curves are shifted logarithmically progressively downwards for better visibility, so that the spectral shape is preserved even though the flux density scale is not. The curves are shifted by the following factors: 2004.7 by 0.80, 2005.0 by 0.60, 2005.3 by 0.50, 2006.2 by 0.25, 2006.4 by 0.15, and 2007.6 by 0.10. The uncertainties are estimated standard errors, including statistical and systematic contributions. The data include both our own and re-reduced archival data (see Table 2).

of the center of the shell in each of the four phase-referenced, 5-GHz images shown in Figure 3. We then averaged these four sets of coordinates and use the average to represent the coordinates of the shell center and the explosion center position, which is $\text{Ra} = 02^{\text{h}} 22^{\text{m}} 31^{\text{s}}.321457$, $\text{decl.} = 42^{\circ} 19' 57''.25951$. We note that a minimum uncertainty in this center position can be derived from the scatter of the individual estimates, and is $\sim 60 \mu\text{as}$ and $\sim 180 \mu\text{as}$ in RA and decl. respectively, and we estimate realistic uncertainties in the actual position of the center of the shell the order of $200 \mu\text{as}$. We note that the largest component of this uncertainty is not astrometric, but comes from the difficulty of identifying the center position of the shell in the

morphology, and our measurements of proper motion below do not depend on this estimate of the position of the shell's center.

We discuss the images in turn:

a) 5 GHz, 1999 Feb. 21: (Fig. 3a) The northeast bright spot dominates. There is a suggestion that it has an extension towards the center. A version of this image was previously published in Bietenholz et al. (2002).

b) 5 GHz, 2002 Nov. 10: (Fig. 3b) The northeast bright spot continues to dominate the image. Again, a slight extension towards the center is seen, but it cannot be clearly identified as the central bright spot. A version of this image was previously published in Bietenholz et al.

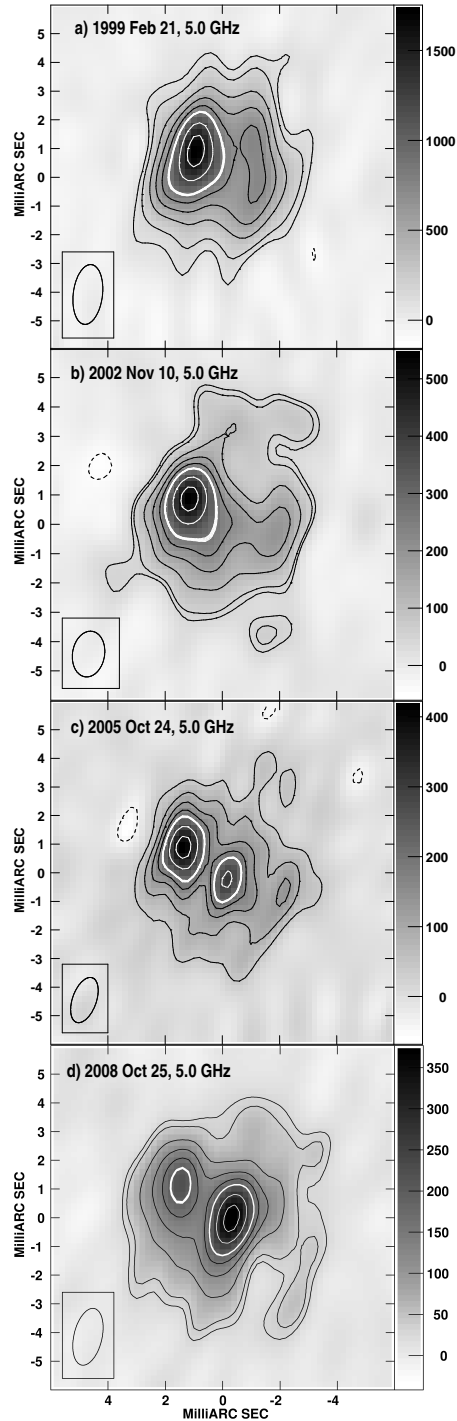


Figure 3. A sequence of VLBI images of SN 1986J at 5 GHz, showing its evolution over the last decade. In each panel, the coordinate system is centered on the estimated position of the center of the shell ($02^{\text{h}} 22^{\text{m}} 31^{\text{s}}.321457$, $42^{\circ} 19' 57''.25951$, see text). The contours are in % of the peak brightness, with negative ones being dotted. Each panel has contours at 10, 20, 30, 40, **50**, 70, and 90%, with the 50% one being emphasized and the lowest white one. The lowest contours, given for each panel below, are three times the rms background brightness. The FWHM size of the convolving beam is indicated at lower left in each panel. North is up and east is to the left. This figure is also available as an mpeg animation in the electronic edition of the *Astrophysical Journal*. a) 1999 Feb 21, 5 GHz. The peak brightness was $1720 \mu\text{Jy beam}^{-1}$, the lowest contour 5.5%, the rms background brightness $31 \mu\text{Jy beam}^{-1}$, and the convolving beam 2.09×1.02 mas at p.a. -7° . b) 2002 Nov 10, 5 GHz. The peak brightness was $543 \mu\text{Jy beam}^{-1}$, the lowest contour 7.6%, the rms background brightness $14 \mu\text{Jy beam}^{-1}$, and the convolving beam 1.57×1.12 mas at p.a. -10° . The visibility data were tapered slightly in u to increase signal-to-noise and produce a somewhat less elongated beam. c) 2005 Oct. 24, 5.0 GHz. The peak brightness was $414 \mu\text{Jy beam}^{-1}$, the lowest contour 9.3%, the rms background brightness $13 \mu\text{Jy beam}^{-1}$, and the convolving beam 1.65×0.83 mas at p.a. -20° . d) 2008 Oct. 25, 5.0 GHz. The peak brightness was $388 \mu\text{Jy beam}^{-1}$, the lowest contour 7%, the rms background brightness $9.0 \mu\text{Jy beam}^{-1}$, and the convolving beam was 2.02×0.98 mas at p.a. -13° .

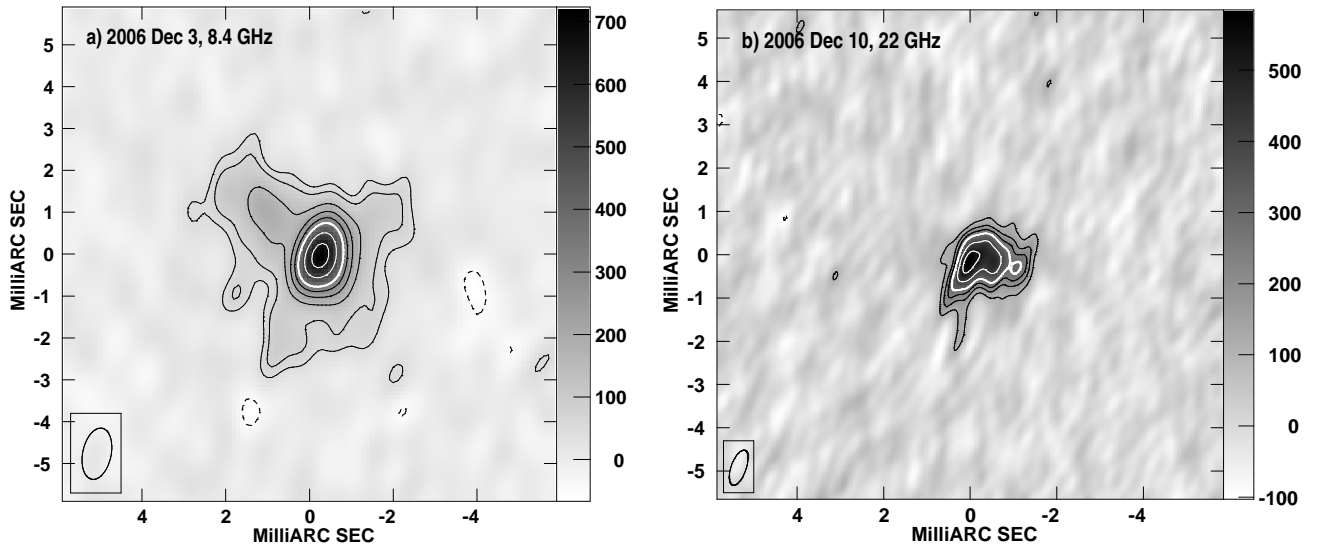


Figure 4. VLBI images of SN 1986J at 8.4 and 22 GHz. In each panel, the coordinate system is centered on the estimated position of the center of the shell ($02^{\text{h}} 22^{\text{m}} 31^{\text{s}}.321457$, $42^{\circ} 19' 57''.25951$, see text). The contours are in % of the peak brightness, with the lowest being at three times the rms background brightness, and the 50% being emphasized and being the first white contour. The FWHM of the convolving beam is shown at lower left. North is up and east to the left. a) Contours are drawn at -6 , 6 , 10 , 20 , 30 , 50 , 70 , and 90% of the peak brightness, which was $717 \mu\text{Jy beam}^{-1}$. The rms background brightness was $15 \mu\text{Jy beam}^{-1}$, and the convolving beam FWHM was 1.24×0.68 mas at p.a. -12° . b) Contours are drawn at -17 , 17 , 30 , 50 , 70 , and 90% of the peak brightness, which was $580 \mu\text{Jy beam}^{-1}$. The rms background brightness was $34 \mu\text{Jy beam}^{-1}$, and the convolving beam FWHM was 0.85×0.35 mas at p.a. -20° .

(2004a).

c) 5 GHz, 2005 Oct. 24: (Fig. 3c) The central bright spot is now clearly seen at 5 GHz although it is not yet as strong as the northeast bright spot. A version of this image was previously published in Bietenholz & Bartel (2008a).

d) 5 GHz, 2008 Oct. 25: (Fig. 3d) The central bright spot now dominates at 5 GHz, and the northeast bright spot is becoming relatively fainter. The shell continues to expand (see § 3.1 below for a determination of the expansion velocity).

e) 8.4 GHz, 2006 Dec. 3: (Fig. 4a) This run benefited from the newly available 512 Mbits s⁻¹ recording bandwidth. The resulting image is dominated by the central bright spot, with the northeast bright spot and the remainder of the shell being only marginally discernible.

f) 22 GHz, 2005 Apr. 25: This image was very similar to the later 22 GHz image in 2006, discussed below. As it was of notably lower signal-to-noise ratio, we do not reproduce it here (it was reproduced in Bietenholz & Bartel 2008a).

g) 22 GHz, 2006 Dec. 10: (Fig. 4b) At this frequency, the steep-spectrum shell is not visible, and the central bright spot dominates. The latter is now clearly resolved and appears somewhat asymmetrical, with a brightness peak to the east. The finger-like extension to the south is of marginal significance. This image was deconvolved with CLEAN, but we note that maximum entropy deconvolution (AIPS task VTESS) produces a very similar image.

3.1. Expansion

The average expansion velocity and deceleration can be determined from the VLBI data by estimating the size of the supernova at each epoch. As SN 1986J's morphology is becoming increasingly irregular, estimating the size by fitting a simple geometrical model to the visibility data (as we did for SN 1993J, see e.g., Bietenholz et al. 2001; Bartel et al. 2002) is no longer practical. We take as a representative (angular) radius the average radius of the contour which contains 90% of the total flux density in the image. Measures of the radius derived from images are complicated by the convolution of the images by a clean beam, but a consistent estimate of the expansion rate can be obtained by comparing radii derived from images convolved with an approximately co-evolving beam. For a fuller discussion, see Bietenholz et al. (2002), where we showed that the expansion up to 1999 had a power-law form with the radius, $r \propto t^{0.71 \pm 0.11}$. We accordingly use images convolved with a co-moving beam,⁶ whose dimensions scale with $t^{0.70}$. We call this radius $\theta_{90\% \text{ flux}}$.

⁶ This is the same procedure we used in Bietenholz et al. (2002), where we also found that the expansion curve is not sensitive to the exact time-dependence of the restoring beam, as long as it is similar to the time-dependence of the radius. The use of an approximate value for the coefficient of the expansion power-law should therefore not significantly bias our result. Note that the value of 0.70 we use for this coefficient is slightly different from the value of 0.75 that we used in Bietenholz et al. (2002). The present value is a somewhat better match to the fit power-law expansion of the supernova. Note also that our present value of the expansion coefficient is in agreement within the uncertainties with the value we had obtained in Bietenholz et al. (2002), but does not support the higher value of 0.90 ± 0.06 reported by Pérez-Torres et al. (2002).

Table 3 gives the derived radii for our various observing epochs. For observations after 2000, we do not determine radii from the observations at 8 GHz or above because at these frequencies, the shell was not sufficiently distinct for a useful measurement. We further note that the increasingly non-self-similar evolution of the morphology makes such average measures of the radius and expansion less reliable, however, our fit to the expansion should give a reasonable estimate of the properties of the expansion averaged over the entire shell.

We fix the explosion date, t_0 , at 1983.2, the value that we determined in Bietenholz et al. (2002) from both the expansion measurements and the radio light-curve. A least-squares fit of a power-law then gives an average expansion $\theta_{90\% \text{ flux}} \propto t^{0.69 \pm 0.03}$, consistent with, but more accurate than the value we had derived in Bietenholz et al. (2002) for the measurements up to 1999.

We plot the resulting expansion curve in Figure 5. The two radii after epoch 1999 fall slightly below the earlier power-law fit, suggesting a possible slight increase in the deceleration. However, we caution that the increase in brightness of the central bright spot relative to that of the shell might lead to a $\theta_{90\% \text{ flux}}$ being a slight underestimate of the true radius of the shell.

The average expansion velocity measured between the 1999 and 2008 epochs was $5700 \pm 1000 \text{ km s}^{-1}$. Although this velocity, based on $\theta_{90\% \text{ flux}}$, is likely not the exact velocity of the outer radius of the shell of radio emission, it should be a reasonable approximation thereof.

3.2. Positions and Proper Motion of the Two Bright Spots

How does the expansion of the supernova compare with the proper motions of the northeast and central bright spots? Since our images are phase-referenced to the brightness peak of the un-related nearby compact radio source, 3C 66A, we can accurately determine the proper motion of the two bright spots relative to 3C 66A.

Before we proceed to the proper motions, we briefly discuss the uncertainties which will apply to such measurements (for other discussions on the astrometric accuracy obtainable with VLBI, see Bietenholz et al. 2001, 2004b; Pradel et al. 2006). Our estimated astrometric uncertainties below consist of the following three components: 1) An uncertainty due to the noise in the image. 2) An uncertainty in identifying a particular point in the morphology of the reference source, 3C 66A, which is slightly time and frequency dependent⁷. We estimate the latter uncertainty component as $20 \mu\text{as}$ in RA and $70 \mu\text{as}$ in decl., with the decl. component being larger because the source is elongated approximately in the north-south direction. 3) An astrometric uncertainty due to errors in the station coordinates, earth orientation, and tropospheric correction, which we estimate at $30 \mu\text{as}$ in each coordinate (see Pradel et al. 2006).

We first turn to the northeast bright spot. It was clearly detected already in 1999 (Bietenholz et al., 2002; for a similar image from an independent reduction of

⁷ Kovalev et al. (2008) show that frequency-dependent shifts in core position are common among compact radio sources. For example, see Bietenholz et al. (2004b) and Bietenholz et al. (2000) for measurements of the variability in time and frequency of the compact core of the nearby galaxy M81.

Table 3
Angular Sizes of SN 1986J

Date	Frequency (GHz)	Age ^a (yrs)	Angular Size ^b (mas)
1988 Sep 29	8.4	5.55	1.37 ± 0.10^c
1990 Jul 21	8.4	7.35	1.83 ± 0.10^c
1999 Feb 22	5.0	15.94	3.07 ± 0.10^c
2002 Nov 10	5.0	19.66	3.60 ± 0.14
2005 Oct 24	5.0	22.62	3.71 ± 0.15
2008 Oct 26	5.0	25.62	4.23 ± 0.17

^a The explosion date is not precisely known. We use a best-fit explosion epoch of 1983.2 determined in Bietenholz et al. (2002).

^b We take as a representative angular radius $\theta_{90\% \text{ flux}}$, which is the average radius of the area containing 90% of the clean flux density in the image. The images are convolved with an approximately co-moving restoring beam. See text for details.

^c These values are from data discussed in Bietenholz et al. (2002), although the present values of $\theta_{90\% \text{ flux}}$ differ slightly from the ones reported there because we are using a slightly different co-moving convolving beam. In that earlier reference, we used a convolving beam whose size increased $\propto t^{0.75}$, whereas the present values are based on a beam whose size increases $\propto t^{0.70}$, which better matches the actual expansion of the supernovae. The difference in derived radii are small, with the values of $\theta_{90\% \text{ flux}}$ changing by less than their stated uncertainties.

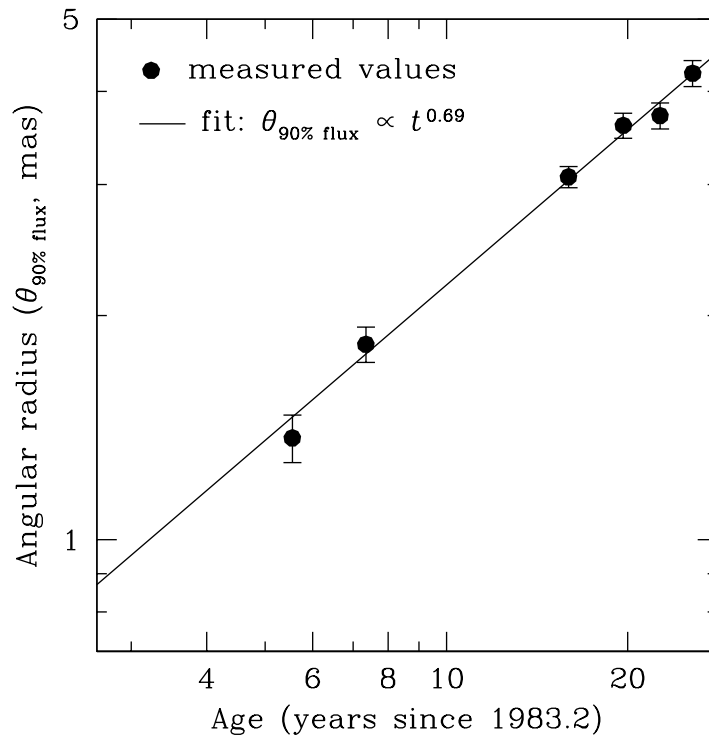


Figure 5. The expansion curve of SN 1986J. We plot the angular outer radius, $\theta_{90\% \text{ flux}}$ (the angular radius which contains 90% of the total flux density in the image, see text, § 3.1 for details), against the age, both on logarithmic scales. The line indicates expansion of the form $\theta \propto (t - t_0)^m$, with $m = 0.69$, where $t = 0$ corresponds to the fixed epoch 1983.2, which was the best weighted least-squares fit to the points plotted.

our observations, see Pérez-Torres et al. 2002). We find that, based on a linear fit to the position in the 1999 Feb., 2002 Nov., 2005 Oct., and 2008 Oct. images at 5 GHz, the proper motion of the northeast bright spot was $60 \pm 20 \mu\text{as yr}^{-1}$, corresponding to a speed of $3000 \pm 1000 \text{ km s}^{-1}$, 2400 ± 250 and $1500 \pm 700 \text{ km s}^{-1}$, in RA and decl. respectively.

Does the current proper motion of the northeast bright

spot place it at the explosion center at the time of explosion? To answer this question requires knowing the position of the explosion center. As mentioned earlier, this center is not accurately known for SN 1986J, but as an estimate we use the average position of the center of the shell, as described in § 3 above. Extrapolating the northeast bright spot's present proper motion the explosion epoch of 1983.2 yields a position consistent with

the estimated center position within 1.9 and 0.8 sigma in RA and decl., respectively. If allowance for deceleration is made, then the spot's 1983.2 extrapolated position is even closer to the center. In fact, a radial motion with the same power-law dependence on time as the overall expansion, which has $r \propto t^{0.69}$, is compatible with our measurements, as can be seen in Figure 6, where we show the radial motion of the northeast bright spot.

A homologous, power-law expansion which includes the northeast bright spot is therefore consistent with our measurements, with the spot's present position and proper motion being compatible with it being at the center of the shell at the explosion epoch. We note, however, that the uncertainties are not small, so considerable deviation from the power-law expansion, for example stronger deceleration, or motion with a constant speed, are also consistent with our measurements.

We turn now to the central bright spot. It is best defined in the images from 2003 June 22 (15 GHz, Bietenholz et al. 2004a), 2006 Dec. 10 (22 GHz) and 2008 Oct. 26 (5 GHz). If we estimate the center bright spot's position at each epoch by the position of the brightness peak, we can determine the spot's proper motion. A linear fit to the three positions gives a proper motion of +4 and +31 $\mu\text{as yr}^{-1}$ in RA and decl., respectively. The morphology of the bright spot makes the peak brightness position somewhat resolution-dependent, (and possibly frequency-dependent), and we estimate that the accuracy with which any particular spot in the morphology can reliably be identified to be on the order of 100 μas . In addition to the other uncertainties estimated above, we use a rounded value of 120 μas for the uncertainty in the spot position in each coordinate, which leads to an uncertainty in the proper motion of 31 $\mu\text{as yr}^{-1}$ in each coordinate. This implies a speed of $1500 \pm 1500 \text{ km s}^{-1}$ at 10 Mpc. The estimate of the proper motion is consistent with the central bright spot being stationary. The average position of the central bright spot is $300 \pm 150 \mu\text{as}$ from the geometric center of the shell (see § 3). However, given the uncertainty in associating the explosion center with the geometric center of the shell, we only say that the position of the central bright spot is marginally consistent with that of the explosion center.

3.3. Brightness Evolution of the Two Bright Spots

In order to quantify the evolution of the brightness of the northeast and central bright spots, we fitted simple models to each bright spot in the image plane. In particular, in the region near each spot we fit an elliptical Gaussian of the same dimensions as the restoring beam, i.e., the equivalent of a point source, and a baseline level.

Although the assumptions that the bright spots are in fact unresolved and that they can be separated in this way are not unquestionable, we feel that this procedure gives a reasonable approximation of the relative flux density of the two spots at each epoch, and is more accurate than, for example, relying only the spot's peak brightness.

In Figure 7 we show the 5-GHz evolution of the flux density of each bright spot relative to the total flux density in the image as a function of time. The northeast bright spot's relative brightness increases, reaching a maximum of $\gtrsim 20\%$ of the total flux density at an age of ~ 16 yr, and fades thereafter. Recall, how-

ever, that the total flux density is decreasing relatively rapidly as a function of time (§ 2.2, Figure 1), so in absolute terms, the brightness of the northeast bright spot decreases monotonically. At its relative peak, its flux density was $\sim 1.3 \text{ mJy}$, and its radio luminosity, assuming an $\alpha = -0.61$ spectrum up to 100 GHz, was $\sim 6 \times 10^{36} \text{ erg s}^{-1}$.

The central bright spot was not clearly visible (at 5 GHz) till age 22.6 yr, but by age 25.6 yr, it had increased to $\sim 15\%$ of the total flux density. The central bright spot is still increasing in brightness in absolute terms, but the absolute increase is not as rapid as the relative one plotted in Figure 7. In 2008, the central bright spot had a flux density of $\sim 390 \mu\text{Jy}$, and a radio luminosity of $\sim 2 \times 10^{36} \text{ erg s}^{-1}$ (again assuming a spectrum with $\alpha = -0.61$ up to 100 GHz).

4. DISCUSSION

4.1. Overall Evolution: Expansion Curve, Deceleration, and Spectral Index

The expansion curve in Figure 5 is compatible with a power-law expansion, and earlier we found the best fit to correspond to $r \propto t^{0.69}$. The flux density decay, however, shows a distinct change in the power-law slope at some time between 1989 and 1995, i.e., between ages of 6 to 12 yr (Bietenholz et al. 2002). Unfortunately no flux density measurements are available in this period to determine the time of change more accurately. Similar behavior was found for SN 1993J with a steepening of the flux density decay at $t \sim 7$ yr (Bartel et al. 2002; Weiler et al. 2007). In the case of SN 1993J, this steepening was found to correspond to a decrease in deceleration (Bartel et al. 2002). This is the general behavior expected when there is a relative decrease in the CSM density. Is a similar behavior seen in SN 1986J? Examining the expansion curve in Figure 5 (see also expansion curves including earlier points in Bietenholz et al. 2002, 2005) suggests that a significant *decrease* in deceleration in the age range of 6 to 12 yr is not compatible with the data, although a small *increase* in deceleration might be. This would suggest that the increase in the rate of flux density decay is due not to a relative decrease in the CSM density but rather to one in the ejecta density. This suggests a steep density profile in the ejecta in the exterior regions, with a somewhat flatter profile in the interior. Such a flattening is indeed expected from models of supergiant stars (see, e.g., discussion in Chevalier 2005). Although suggestive, we do not regard this result as definitive because the measurements do not demand any break in the power-law expansion curve.

The evolution of the integrated spectrum is complex, but at low frequencies the spectrum seems to have a power-law shape. One can with reasonable confidence associate the part of the spectrum at the lowest frequencies with the shell, with the complex evolution due to the emergence of the central bright spot being restricted to higher frequencies ($\gtrsim 5 \text{ GHz}$). As we showed in § 2.3 above, the lowest part of the spectrum seems to be initially rather steep, with $\alpha = -0.67$, then by 1995 it flattens somewhat to $\alpha = -0.44$, and subsequently it steepens again.

What could cause such a variation of the radio emission spectrum with time? Since the emission spectrum of

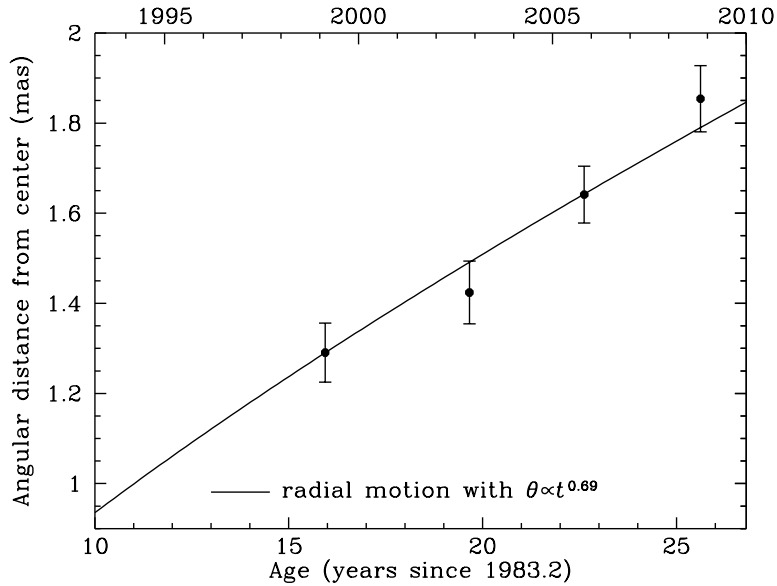


Figure 6. The angular distance of the northeast bright spot from the center as a function of time. The additional axis labels along the top give the calendar year. The spot's angular distance is taken to be that between the spot local maximum and the estimated explosion center (see text, § 3.2, for details on the estimation of the explosion center). The shell expands with outer angular radius $\propto t^{0.69}$ (see text § 3.1). Of the possible expansion curves which have $\theta \propto t^{0.69}$, we show as the solid line the one that best matches the spot's motion. Note that the spot's displacement as a function of time is somewhat dependent upon the choice of the explosion center, although for reasonable choices, the nature of the expansion curve remains unchanged. Our plotted error bars are the uncertainty in the spot position and an estimated uncertainty of 0.1 mas in the explosion location added in quadrature. The spot's motion is consistent with homologous expansion.

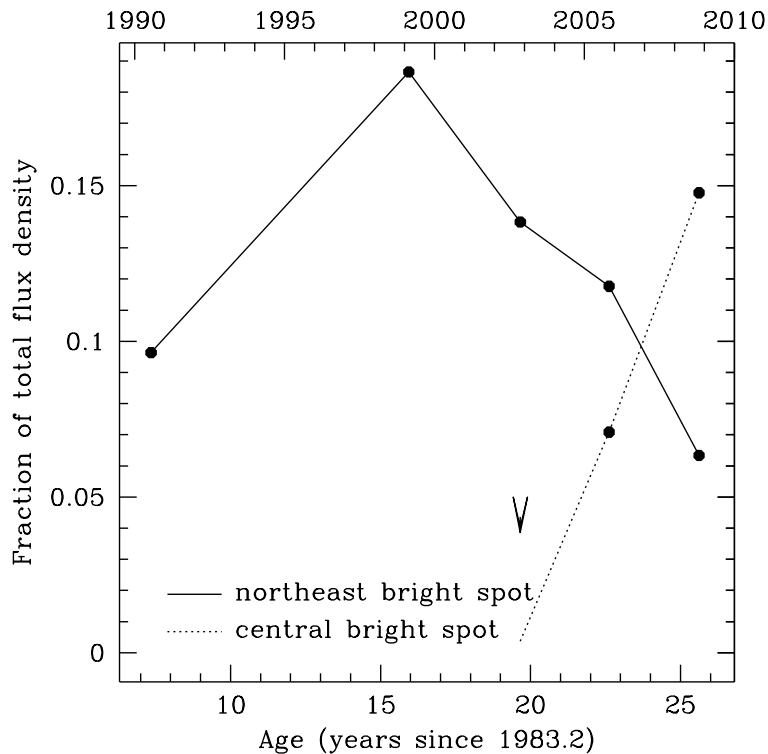


Figure 7. The evolution at 5 GHz of the fractional flux density of the bright spots in the northeast and in the center of the projected shell as a function of time. The additional axis labels along the top give the calendar year. The bright spot flux densities are estimated by fitting, by least squares, a point source and a baseline level in the region near the spot. The fraction of the flux density is taken to be the fitted flux density for the point source divided by the total CLEAN flux density in the image. For the first three epochs, the bright spot in the center is not discernible. The chevron shows an upper limit on the central bright spot flux density at age 19.7 yr, which we derived by taking half the surface brightness at its location.

synchrotron radiation reflects the energy spectrum of the relativistic particles, one obvious interpretation is that the latter energy spectrum is also changing with time, perhaps in response to varying conditions at the shock front where the particle acceleration occurs. However, optical depth effects also offer a possible explanation. Although most of the radio-emitting shell is optically thin at cm wavelengths, the interior of the shell is not expected to be so because of the high density of thermal material. If mixing is occurring, a substantial transition zone between the optically thin shocked material and the optically thick ejecta may exist, which could partly absorb the radio emission from a substantial fraction of the shell, and thus modify the integrated spectrum. In fact, the slow turn-on of the lightcurve suggests a significant amount of absorption mixed in with the radio emission already at early times (Weiler et al. 1990).

We note that changes with time in the radio spectral index are seen in other supernovae. In particular, a flattening with time of the radio spectrum as seen for SN 1993J (Bartel et al. 2002)⁸ and at least at the latest times also for SN 1979C (Bartel & Bietenholz 2008), may be characteristic of the evolution of radio supernovae, and could be coupled with a steepening of the lightcurve decay.

4.2. Comparison of Expansion Curve to Optical Radial Velocities

From our VLBI measurements, we determined the expansion velocity of the edge of the radio emission region in the plane of the sky. Since the forward shock forms the outer boundary of the region where radio emission is expected to occur, our VLBI expansion velocity can be reasonably associated with the velocity of the forward shock velocity (see discussion on this subject for SN 1993J in Bartel et al. 2007). Note that since the geometry of SN 1986J is somewhat irregular, the assumption of sphericity which allows a comparison of the velocities in the sky-plane measured with VLBI with those along the line-of-sight measured from optical spectra is likely true only to first order.

In the optical, there are a number of spectral lines present which allow radial velocity measurements. Recently, Milisavljevic et al. (2008), obtained new optical spectra at epoch 2007.7, and compared them to earlier ones from 1989.7 and 1991.8. The optical emission lines are thought to mainly come from two distinct locations. Narrow optical lines, chiefly H α , He I and [N II] λ 5755, are thought to originate in dense, shock-heated circumstellar medium, and therefore have relatively narrow line-widths, typically $< 2000 \text{ km s}^{-1}$. These lines were more prominent early on and have faded since 1989.

Currently the most prominent emission lines are the [O I] $\lambda\lambda$ 6300, 6364 and [O II] $\lambda\lambda$ 7319, 7330 forbidden lines of oxygen, with the [O III] $\lambda\lambda$ 4959, 5007 line also being discernible. In 1989.7, these lines showed a double-peaked structure, with one peak at a velocity of -1000 km s^{-1} (relative to the systemic one), and the

other near -3500 km s^{-1} , and the maximum velocity, on the blue sides of these lines, was $\sim -6000 \text{ km s}^{-1}$. Similar velocities were seen in 1991.8. By 2007.7, the double structure was less clearly discernible, the maximum blue velocity had decreased and the [O III] line had almost vanished. Milisavljevic et al. (2008) attribute these forbidden lines to ejecta which has been heated (but not yet shocked) by the reverse shock.

This interpretation of the optical lines is consistent with the expansion velocities measured in the radio. In 1989.7, the forward shock velocity was $\sim 8300 \text{ km s}^{-1}$, and the reverse shock velocity would be expected to be about 80% of this, or $\sim 6600 \text{ km s}^{-1}$. The velocities implied by both the line-center and the total widths seen in the forbidden oxygen lines are consistent with being inside the reverse shock in 1989.7. By 2007.7, the forward shock velocity is $\sim 5500 \text{ km s}^{-1}$, and the expected reverse shock velocity $\sim 4400 \text{ km s}^{-1}$. The evolution of the optical line profiles is consistent with this reduction in the velocity of the reverse shock in that, particularly for the [O II] line, with the highest (blue) velocities now being $\sim -4300 \text{ km s}^{-1}$. This suggests that, of the ejecta responsible for the oxygen forbidden line emission, the highest velocity fraction passed through the reverse shock between 1989.7 and 2007.7, and the remainder is now situated relatively close to the reverse shock.

4.3. Magnetic Field

The magnetic field can be estimated from the radio brightness and the source size using minimum energy arguments (Pacholczyk 1970)⁹. Given that the spectrum shows deviations from a power-law, we will perform the calculation only for the shell component, which dominates below $\nu = 5 \text{ GHz}$ and is observed to have a power-law spectrum with an average $\alpha = -0.5$ (§ 2.3). The derived field strength depends on the ratio, k , of energies of relativistic protons and electrons. We use a value of $k = 100$, as was found to be reasonable for strong shocks in supernova remnants by Beck & Krause (2005). We estimate first the field strength in the shell, for which we use the angular radii derived in § 3.1 above, and we take the flux density at 1.4 GHz to be representative of the shell (as opposed to that of the central bright spot).

Using the values from 1988 to 2008, we find that B has an approximate power-law dependence on time and radius, as might be expected from the approximately power-law evolution of both the flux density and radius. In particular, we find that for minimum energy, $B \simeq 60 (t/10 \text{ yr})^{-1.3} \text{ mG}$, and that $B \propto r^{-1.8}$ for $t > 1500 \text{ d}$. Although such estimates of the field are uncertain by factors of several, the estimates of its dependence on t and r are likely to be somewhat better constrained with the exponents being uncertain by perhaps $\sim 70\%$.

4.4. The Mass Loss Rate of the Progenitor

⁹ We note that Beck & Krause (2005) point out a number of shortcomings in the standard formulae of Pacholczyk and give revised formulae. However, for relatively flat spectra, the differences between the standard and revised formulae are not large and only weakly dependent on the field strength, so a field calculated using the revised formula would have almost the same dependence on time and radius. In the interests of easier comparison with earlier results we estimate our magnetic field using the standard formula from Pacholczyk (1970).

⁸ Chandra et al. (2004) also find a flattening with time of the optically-thin spectrum of SN 1993J. A slight but systematic flattening is also visible in the plotted data after $t = 500 \text{ d}$ of Weiler et al. (2007), although they fitted a model with a constant spectral index for the optically thin part of the spectrum.

Can we estimate the mass-loss rate of the progenitor from our observations? This mass-loss rate is often estimated from studies of the radio lightcurves. It is determined mostly by the rising part of the lightcurve, while the emission is optically thick, and is usually expressed as \dot{M}/v_w , where v_w is the wind velocity. However, such calculations can significantly overestimate the value of \dot{M}/v_w (see, e.g., Bartel & Bietenholz 2003), and in general have been shown to be somewhat problematic if not based on complete physical models (e.g., Fransson & Björnsson 2005). In particular, in the case of SN 1986J, Weiler et al. (1990) cited a value of $\dot{M}/v_w = 2.4 \times 10^{-4} M_\odot \text{ yr}^{-1}$ (for $v_w = 10 \text{ km s}^{-1}$), based not on the rising part of the lightcurve, but rather on a short term variation in the optical depth seen in late 1988. Later, Weiler et al. (2002) reported a notably lower value of $4.3 \times 10^{-5} M_\odot \text{ yr}^{-1}$, which is based on a model involving clumpy absorption in the CSM. Houck et al. (1998) suggest a value of a few times $10^{-4} M_\odot \text{ yr}^{-1}$ based on X-ray observations. In any case, given the departures from self-similarity and the considerable evidence of clumpiness in the CSM, which will have a strong effect on both radio brightness and absorption, any estimated mass-loss rate is likely to be quite uncertain.

A mass-loss rate between 4×10^{-5} and, say, $3 \times 10^{-4} M_\odot \text{ yr}^{-1}$ with $v_w = 10 \text{ km s}^{-1}$ would imply that by age 25.6 yr (2008.8), when the radius of the shock-front is $6.3 \times 10^{17} \text{ cm}$, the swept-up mass would be $0.8 \sim 6 M_\odot$. For this range in mass-loss rate, the kinetic energy of the swept-up mass would be $(0.2 \sim 1.7) \times 10^{51} \text{ erg}$ ($v \simeq 5400 \text{ km s}^{-1}$). Since the kinetic energy of the swept-up mass can be at most a fraction of the original kinetic energy of the ejecta, which was likely not much larger than 10^{51} erg (e.g., Jones et al. 1998), we regard the higher end of this mass-loss range as unlikely on energetic grounds. We therefore estimate a present swept-up mass of $0.8 \sim 2 M_\odot$, and an average mass-loss rate (\dot{M}/v_w) in the range of $(4 \sim 10) \times 10^{-5} M_\odot \text{ yr}^{-1}$. Such a range of mass-loss rate implies a CSM density at the 2008.8 outer shock radius of $6.3 \times 10^{17} \text{ cm}$ of $(5 \sim 13) \times 10^{-22} \text{ g cm}^{-3}$. If we assume that the fraction of hydrogen atoms is 75% of the total, then the hydrogen number density is between $230 \sim 570 \text{ cm}^{-3}$.

4.5. The Northeast Bright Spot

The images are characterized by two bright spots, whose flux densities vary. The first one, in the northeast, appears to be a component of the shell. It was first clearly discernible at age ~ 16 yr, although it may have been present already earlier. Its proper motion is consistent with homologous expansion with the bulk of the shell (Fig. 6). As can be seen in Figure 7, at its peak relative brightness (age ~ 16 yr) approximately $\sim 20\%$ of the total flux density originates from this spot. Unfortunately, our observations do not constrain the relative lightcurve around the time of the peak precisely, the peak relative brightness may have been as high as $\sim 30\%$ of the total, although it must have occurred between our 1990 and 1999 epochs. The northeast bright spot appears marginally resolved in our images. On 2005 Oct. 24 our FWHM resolution was $1.65 \times 0.83 \text{ mas}$, so the spot's angular diameter must have been $\sim 1 \text{ mas}$, corresponding

to 14% of the shell's outer diameter, or $1.5 \times 10^{17} \text{ cm}$.

Since the northeast bright spot appears to be part of the projected shell, the most plausible interpretation is that it is due to the ejecta interacting with a dense clump in the CSM. This would account for the relative brightness of the spot first increasing and then falling off. In fact, the relative lightcurve of the northeast bright spot in Figure 7 suggests that the shock has traversed the bulk of the clump between ages 10 to 20 yr. Our expansion curve suggests that, on average around the circumference, the shock travelled a distance of $2 \times 10^{17} \text{ cm}$ during this time, in reasonable agreement with the clump diameter estimated above.

If we assume both the dense clump and the outer shock to be spherical, with the clump having the dimensions estimated above, then, when the shock is midway through the clump, $\sim 1\%$ of the outer shock front area is interacting with the dense clump. Since the radio emission is driven by the shock, we will consider the radio luminosity per unit area of the shock, and we will further assume that the radio luminosity scales as the 5-GHz flux density. The northeast bright spot at its peak emitted about one quarter of the 5-GHz flux density of the remainder of the shell. We can therefore calculate that the region in the dense clump must be ~ 25 times brighter than the remainder. Our proper motion measurements show that the velocity of the shock in the clump is approximately the same as it is for the remainder of the shell, so the radio luminosity per unit area of the shock should scale with the CSM density¹⁰. We found above (§ 4.4) that the present average CSM density was $(5 \sim 13) \times 10^{-22} \text{ g cm}^{-3}$, suggesting that the densities in the clump are $(1.3 \sim 3.2) \times 10^{-20} \text{ g cm}^{-3}$, corresponding to hydrogen number densities of $5800 \sim 14,000 \text{ cm}^{-3}$, giving the clump a total mass of $0.01 \sim 0.03 M_\odot$. We note, however, that these densities represent an average over the clump, and much higher densities in parts of the clump are not excluded by the radio data.

There are a number of other indicators pointing to the existence of such dense clumps in the CSM of SN 1986J. First, the very high Balmer decrement (Rupen et al. 1987), and other features in the late-time spectra (Milisavljevic et al. 2008), suggest the presence of very high number densities ($> 10^6 \text{ cm}^{-3}$). Second, the slow rise of the radio lightcurve is interpreted as also implying a very clumpy CSM (Weiler et al. 1990). Third, because the H α line, which has a width of only $\sim 1000 \text{ km s}^{-1}$ (e.g., Milisavljevic et al. 2008; Leibundgut et al. 1991), is far too narrow to arise from the ejecta near the forward shock ($v \sim 5700 \text{ km s}^{-1}$; § 3.1), it has been suggested that most of the H α emission is coming not from the ejecta, but rather from shocked, dense clouds in the CSM resulting from a very clumpy wind from the progenitor star (Chugai & Danziger 1994;

¹⁰ The radio luminosity is thought to scale with the post-shock energy density (e.g., Chevalier 1998, 1982). In the absence of absorption, the radio luminosity will depend on the fractions of the post-shock energy which go into the magnetic field and into accelerated particles. There is no solid ground for thinking that these fractions are constant, indeed they are likely to vary somewhat both as a function of shock velocity and the density and chemical composition of the CSM. It is likely, however, that these variations are relatively small, whereas the variation in the CSM density can be several orders of magnitude or more.

Chugai 1993).

Red supergiant stars of mass 20-40 M_{\odot} are known to have episodes of strong mass loss, resulting in large density contrasts in the CSM. For example, Smith et al. (2001, 2009) show that the red supergiant VY Canis Majoris (mass 20-40 M_{\odot}), which is likely similar to the progenitor of SN 1986J, is surrounded by a nebula produced by rapid mass loss ($2 \sim 4 \times 10^{-4} M_{\odot} \text{ yr}^{-1}$). This nebula, which extends out to a radius of $\gtrsim 10^{17}$ cm, similar in scale to the CSM required for SN 1986J, is highly structured with knots and filamentary arcs, which are distributed in an asymmetric way. Smith et al. (2001) argue that the structures in the wind were produced by ejection events which were localized on the stellar surface. For VY Canis Majoris then, and by implication also for other red supergiants, the evidence seems to suggest that the winds can be highly structured, with large density contrasts on small spatial scales. Exactly such structure seems to be required to reproduce the radio emission from SN 1986J.

4.6. The Central Bright Spot: Is It Emission from the Compact Remnant of the Supernova Explosion?

What is the nature of the central bright spot — is it the emission associated with a neutron-star or black-hole compact remnant of the supernova explosion? The first question would be whether the central bright spot is positionally coincident with the explosion center. As we showed in § 3.2 above, the position of the central bright spot is in fact compatible with being in the center of the shell, and its proper motion is consistent with being stationary with respect to the shell. Note that the expansion speed of the shell is much larger than the peculiar velocities of stars and even of pulsars, which latter have a velocity dispersion of $200 \sim 300 \text{ km s}^{-1}$ in the Galaxy (e.g., Hobbs et al. 2005; Lyne & Graham-Smith 1990), so the effect of any peculiar motion of the progenitor or any “kick” received in the explosion would be small and the compact remnant would be expected to remain essentially in the center of the shell over the ~ 25 yrs since the supernova explosion. In this respect, our position and proper motion measurements for the central hot spot are consistent with the expectations for a black-hole or neutron star compact remnant.

We first noted the inversion in the integrated radio spectrum in Bietenholz et al. (2002), and we showed in Bietenholz et al. (2004a) that the inversion in the integrated spectrum was in fact associated with the central bright spot, with the shell and the northeast bright spot discussed above having a simple power-law spectrum as is usually seen in supernovae. In § 2.2 and Figure 2 above we show that both the inflection and the high-frequency turnover points in the radio spectrum are progressing downwards in frequency as SN 1986J ages. The inverted spectrum of the central bright spot suggests partly absorbed radio emission. An opacity decreasing due to the expansion would cause the observed progression to lower frequencies of both the inversion and high-frequency turnover points.

We argued in Bietenholz et al. (2005) that the absorption is probably due to free-free absorption rather than to synchrotron self-absorption (SSA). In fact, our latest 22 GHz images, where the central bright spot is somewhat resolved, largely rules out SSA on the following

grounds. Examination of the image (Fig. 4b) suggests a size of $\gtrsim 1 \times 10^{17}$ cm for the central bright spot. The radius below which SSA would be important, R_p , can be calculated following Chevalier (1998):

$$R_p = 8.8 \times 10^{15} \kappa^{-1/10} \left(\frac{f}{0.5} \right)^{-1/19} \left(\frac{F_p}{\text{Jy}} \right)^{9/19} \\ \times \left(\frac{D}{\text{Mpc}} \right)^{18/19} \left(\frac{\nu}{5 \text{GHz}} \right)^{-1} \text{ cm}$$

where F_p is the flux density at the spectral peak, κ is the ratio of relativistic electron energy density to magnetic energy density, D is the distance, and f is the filling factor. Assuming equipartition ($\kappa = 1$) and substituting our values of $F_p = 3.8 \text{ mJy}$ at $\nu_p = 14 \text{ GHz}$ (2007.6), we obtain $R_p \simeq 1 \times 10^{16}$ cm, which is far lower than the size determined from the image of $\gtrsim 1 \times 10^{17}$ cm, thus effectively ruling out significant SSA at our observing frequencies.

The appearance of the central bright spot at a time long after the supernova’s integrated radio spectrum was optically thin at cm wavelengths suggested that any remaining absorption due to the circumstellar material was minimal. It was natural, therefore, to assume that the absorption seen for the central bright spot was due to un-shocked material interior to the shocked shell, rather than to the CSM. With this assumption, the central bright spot’s likeliest physical location was in the center of the shell, and its most likely interpretation was in terms of radio emission associated with the neutron star or black hole expected to have been left behind after the explosion (Bietenholz et al. 2004a, 2005; Bietenholz & Bartel 2008a).

The turnover frequency is approximately equal to the frequency at which the optical depth to free-free absorption, τ , is unity, is given by

$$\nu_{\tau=1} = 0.3 (T_e^{-1.35} N_e^2 dl)^{1/2} \text{ GHz},$$

where T_e is the electron temperature in K, N_e is the number density of electrons in cm^{-3} , assumed constant along the path-length in pc, dl , with $N_e^2 dl$ being the emission measure. Our integrated spectra (Fig. 2) show that the spectral peak due to the central bright spot occurs at $\sim 20 \text{ GHz}$ in 2002.4. If we assume¹¹, a T_e of 10^4 K then $N_e^2 dl$ is $1.1 \times 10^9 \text{ cm}^{-6} \text{ pc}$. By 2007.6, the turnover frequency is $\sim 14 \text{ GHz}$, so $N_e^2 dl = 0.6 \times 10^9 \text{ cm}^{-6} \text{ pc}$.

The temporal dependence of the absorption is consistent with that expected from the gas within the expanding shell. We found that the emission measure decreased by a factor of ~ 2 between 2002.4 and 2007.6. If we assume the system is expanding homologously, then the density within the shell is proportional to r^{-3} and $N_e^2 dl \propto r^{-5}$. If we further take $r \propto t^{0.69}$ as we found for the shell, we would expect $N_e^2 dl$ to be $\propto t^{-3.45}$, which would lead to a decrease by close to the observed factor of 2 between 2002.4 and 2007.6.

We note, however, that the inverted part of the spectrum is much flatter than is expected from free-free absorption, which produces spectra with an exponential

¹¹ Although T_e is not well known, and can vary strongly with radius, this is probably a reasonable value for radii $> 1 \times 10^{17} \text{ cm}$ (see, e.g., Lundqvist & Fransson 1988).

cutoff at low frequencies. Such flatter spectra below the turnover are produced when a range of different optical depths is present. This suggests that the absorbing material is somewhat fragmented, with some lines of sight having much lower optical depths than others. Indeed, fragmentation of the ejecta is not surprising, since there are a number of instabilities operating in the expanding shell of ejecta (e.g., Gull 1973; Jun & Norman 1996; Chevalier & Blondin 1995), which are expected to lead to fragmentation. If the central bright spot is due to a pulsar, then further instabilities occur when the young pulsar’s wind nebula expands into the supernova ejecta (e.g., Bandiera et al. 1983; Chevalier & Fransson 1992).

As we have shown, the absorption of the radio emission from the central bright spot is consistent with what might be expected from the intervening material in the shell and its observed expansion rate. This suggests that the integrated spectrum above the turnover point shows the intrinsic, un-absorbed spectrum of the central bright spot. In fact, the integrated spectra in Figure 2 show that the spectral index above the turnover point is very similar to that below the inversion point. So, the intrinsic spectral index of the central bright spot is also similar to that of the shell.

If the central bright spot were in fact in the physical center of the shell and represented radio emission associated with the compact remnant of the supernova — either a black hole or a neutron star — then it would be somewhat of a coincidence for its radio emission to have a similar spectral index as that of the shell emission. In particular, if the central bright spot were the wind nebula (PWN) around a very young pulsar, then one might expect it to have a somewhat flatter spectral index, as most PWNe have spectral indices in the range -0.3 to 0.0 (Gaensler & Slane 2006) and as there are no filled-center remnants in the catalog of Green (2004) which have broadband radio spectra steeper¹² than $\alpha = -0.3$. In particular, the youngest known PWNe, the Crab Nebula and G21.5–0.5, have rather flat radio spectra with spectral indices of -0.27 (Bietenholz et al. 1997) and $+0.08$ (Bietenholz & Bartel 2008b), respectively. The observed steep spectrum of the central bright spot, therefore, would not seem to favor the hypothesis of a young PWN. However, an only 27-yr old PWN may not be comparable to the much older known PWNe, so the observed steep spectrum does not rule out a young PWN.

Alternatively, if the central bright spot represents emission from jets emanating from a black hole environment, the radio spectrum is consistent with the expectations but the radio luminosity is not. The possible presence of both self-absorbed and optically thin components in the jet can give rise to both flat and steep spectra, so the observed spectrum can easily be accommodated. However, SN 1986J’s central bright spot is far more radio-luminous than any known stellar-mass black hole system. In par-

ticular, a “fundamental plane” relationship between the radio and X-ray luminosities and black-hole mass has been observed for black-hole systems of a wide range of masses (see, e.g., Falcke et al. 2004; Ho 2008). The unabsorbed X-ray flux from SN 1986J was measured in late 2003 by Houck (2005) to be $\sim 1.6 \times 10^{-13}$ erg s $^{-1}$. Even with the assumption that all this X-ray flux is due to the central bright spot, the “fundamental plane” relation would suggest radio luminosities for a black-hole system of $\sim 10^{-4}$ of that observed for the central bright spot of $\sim 2 \times 10^{36}$ erg s $^{-1}$ (§ 3.3). However, very little is known about such young black-hole systems, so it is not impossible that they would be far more luminous than expected from the fundamental plane relationship. So again, we must conclude that the radio properties of the central bright spot do not seem to argue strongly for an accreting black-hole system, but neither can they exclude it.

4.7. The Central Bright Spot as a Shell Component?

As we showed in § 4.5 above, the northeast bright spot can naturally be explained as the impact of the shock-front on a dense condensation in the CSM. Could the central bright spot be a similar phenomenon, with the dense condensation being coincidentally located near the projected center of the shell? In this case, an approximate equality of the intrinsic spectral indices of the central bright spot with that of the remainder of the supernova is expected, since usually not much variation of the spectral index around the shell is observed.

As we showed, there is considerable evidence that the CSM of red supergiants and of SN 1986J in particular are quite clumpy, and the northeast bright spot suggests that there is at least one dense condensation in the CSM of SN 1986J. There is no particular reason to only expect a single dense clump in the CSM, so the existence of more than one dense clump seems not unlikely.

The expanding shell impacting on a dense CSM clump would cause a local brightening of the radio emission. Although the bulk of the CSM is optically thin at cm wavelengths, clumps with densities as high as $N_e > 10^6$ cm $^{-3}$, and sizes small compared to the shell diameter, would be expected to have large optical depths for cm-wave radio emission. For example, a clump with a diameter of 5×10^{16} cm, corresponding to an angle of ~ 0.3 mas on our images, and a density of 1×10^6 cm $^{-3}$ would have a free-free optical depth at 8.4 GHz of ~ 30 .

The shock hitting a dense clump will produce localized, bright radio emission, as is seen in the northeast bright spot. However, if the dense CSM clump lies on the near side of the expanding shell, fortuitously near the center in projection, then the optically thick clump itself will in fact block most of this bright radio emission. With time, the clump will become optically thin as it either fragments or as the shock eats through it. This scenario would produce a sequence much like what is seen for the central bright spot: a delayed turn on, dependent on the distance of the clump from the explosion center and its density, with an inverted spectrum expected from free-free absorption, followed eventually by an optically thin decay. At 5 GHz, the brightness of the central bright spot is still increasing, (Fig. 7) so we are still in the rising part of its lightcurve.

If we interpret the central bright spot as emission from

¹² see <http://www.mrao.cam.ac.uk/surveys/snrs> for an updated version of the catalog. The possible exception is Vela X, the central source in the Vela supernova remnant, which is often associated with the PWN. Alvarez et al. (2001) found $\alpha_{0.09\text{GHz}}^{8.4\text{GHz}} = -0.39 \pm 0.03$ for Vela X, indicating a relatively steep spectrum for a PWN. More recently, however, Hales et al. (2004) reported on 31 GHz observations of a strong source near the Vela pulsar that they identify with the PWN, and for which they find a slightly inverted spectrum with $\alpha_{8.4\text{GHz}}^{31\text{GHz}} = +0.10 \pm 0.06$

the shock interacting with such a CSM clump, what can be deduced about the physical conditions in this clump? In our latest image at 22 GHz, we can estimate an angular diameter of the central bright spot of ~ 0.7 mas (FWHM), suggesting a linear diameter of $\sim 1 \times 10^{17}$ cm or 0.03 pc. The turnover frequency at this epoch is ~ 12 GHz. If we take the turnover frequency to be that at which the free-free optical depth is unity, the density of the absorbing clump can be estimated from the electron number density which in turn can be calculated from the emission measure using the equation given in § 4.6 above. If we again assume $T_e = 10^4$ K and a constant N_e , and further assume that the clump's line-of-sight depth is equal to the central bright spot's diameter in the plane of the sky, we can calculate that $N_e \sim 2.5 \times 10^5$ cm $^{-3}$. Again, the presence of significantly higher densities cannot be excluded, but the presence of substantial material at the calculated density seems required. The total mass of such an absorbing clump would be $\sim 0.1 M_\odot$ (assuming full ionization). The swept-up mass in 2008.8 is $0.8 \sim 2.0 M_\odot$ (out to a radius of 6.3×10^{17} cm; see § 4.4), so the mass of the clump represents 13% to 5% of the total swept-up mass.

By comparing the part of the spectrum above 20 GHz with that at low frequencies (see Fig. 2), we can estimate that the unabsorbed radio luminosity of the central bright spot is about twice that of the remainder of the supernova. Note that the unabsorbed luminosity of the central bright spot is currently larger than that of the northeast bright spot, since a substantial fraction of the central bright spot's luminosity is still absorbed, with the turnover frequency currently being ~ 12 GHz. If we again assume that radio luminosity per unit shock area scales only with the CSM density, we can estimate the density of the clump relative to that of the average CSM density as we did for the northeast bright spot (§ 4.5). Using the above clump diameter of 1×10^{17} cm, and a shell outer radius of 6×10^{17} cm (for 2006 Dec.) we find that the spot covers $\sim 0.2\%$ of the shell surface. The clump must therefore be $\sim 1000\times$ denser than the average corresponding CSM. As might be expected, since the central bright spot has a much higher unabsorbed luminosity than the northeast bright spot, the density required for the relevant enhancement of the emissivity is also much higher.

We calculated a representative density of $N_e \sim 2.5 \times 10^5$ cm $^{-3}$ for the central clump above, which suggests a representative average density for the CSM at $r \simeq 6.2 \times 10^{17}$ cm of ~ 250 cm $^{-3}$, which in turn implies a mass-loss rate of $6 \times 10^{-5} M_\odot \text{ yr}^{-1}$ (for $v_w = 10$ km s $^{-1}$) which is consistent with the values derived in § 4.4 above.

As mentioned in § 4.2 above, the oxygen forbidden-line emission seems to be dominated by two dense clumps, both on the near side of the remnant. If the central radio bright spot is due to a CSM clump on the near side of the SN, then also in the radio, there would be evidence for two dense clumps. Could the clumps responsible for radio bright spots be the same as the two clumps seen in the optical emission lines? The association seems unclear, since the radio emission, as we have argued, would be due to dense clumps in the CSM, exterior to the forward shock, while the forbidden-line emission is plausibly attributed ejecta heated by the reverse shock, that is in-

terior to the reverse shock.

While it is conceivable that dense CSM clumps cause distortions first in the forward shock but subsequently also in the reverse shock, which latter could in turn give rise to the bright features seen in the oxygen forbidden lines, any association between the radio bright spots and the oxygen-line features must remain speculative.

All said, we think now that the spectral evolution seen in the new observations make an interpretation of the central bright spot in terms of a second shell component and an interpretation in terms of emission from a PWN or a black-hole environment equally plausible.

5. SUMMARY AND CONCLUSIONS

1. We have obtained new multi-frequency VLA flux density measurements and VLBI images of SN 1986J, showing the evolution of this supernova in the radio.
2. The evolution of the integrated radio spectrum is complex. The spectrum at the lowest frequencies has a spectral index in the range of $-0.7 \sim -0.5$. The spectrum above the high-frequency turnover, presumably the intrinsic spectrum of the central bright spot, is equally steep within the uncertainties.
3. The shell continues to expand. The average expansion speed of the shell between 1999 and 2009 was 5700 ± 1000 km s $^{-1}$. This speed is compatible with continued power-law expansion, with the radius increasing $\propto t^{0.69 \pm 0.03}$. The increase in the rate of flux density decay at $t \sim 7$ yr is likely due to a flattening in the profile of the ejecta profile rather than a steepening in the one of the CSM, as no increase in deceleration is observed.
4. The equipartition magnetic field decreases as the supernova expands, with an approximate value of $B \simeq 60 (t/10 \text{ yr})^{-1.3}$ mG. The dependence on the outer shock front radius is $B \propto r^{-1.8}$.
5. Various estimates of the mass-loss converge to values in the range of $(4 \sim 10) \times 10^{-5} M_\odot \text{ yr}^{-1}$ (for $v_w = 10$ km s $^{-1}$).
6. The VLBI images show two bright spots in addition to the shell-like structure. The first is in the northeast of the shell, while the second is near the projected center of the shell. The flux densities of the spots relative to that of the SN as a whole vary with time, with that of the northeast bright spot increasing till ~ 1999 , and decreasing since, while that of the central bright spot continues to increase.
7. The northeast bright spot is likely due to a dense clump in the circumstellar material (CSM). The bright spot's proper motion is consistent with homologous power-law expansion. Number densities of $N_e \sim 10^4$ cm $^{-3}$ or higher are suggested for the clump.
8. The central bright spot has a partly absorbed radio spectrum, with an intrinsic radio spectrum that is similar to that of the shell. The amount of absorption is decreasing with time.
9. The central bright spot's original interpretation as originating in the physical center of the shell and being emission due to the neutron star or black hole remnant of the supernova is supported by its central position, and its stationarity to within 1σ . The new observations, however, suggest an equally plausible alternative explanation

of the central bright spot being radio emission due to the shell impacting upon a second dense CSM clump, fortuitously located on the near side of the shell close to the projected center. The amount of absorption suggests number densities of $N_e \gtrsim 2.5 \times 10^5 \text{ cm}^{-3}$, $\sim 10^3$ higher than the average density of the CSM.

10. From the VLBI images from 1987 to 2008, we produced a movie showing the supernova's evolution.

The European VLBI Network is a joint facility of European and Chinese radio astronomy institutes funded by their national research councils. We have made use of NASA's Astrophysics Data System Abstract Service. We thank the anonymous referee for his suggestions.

REFERENCES

- Aaronson, M., et al. 1982, *ApJS*, 50, 241
 Alvarez, H., Aparici, J., May, J., & Reich, P. 2001, *A&A*, 372, 636
 Baars, J. W. M., Genzel, R., Pauliny-Toth, I. I. K., & Witzel, A. 1977, *A&A*, 61, 99
 Ball, L., & Kirk, J. G. 1995, *A&A*, 303, L57
 Bandiera, R., Pacini, F., & Salvati, M. 1983, *A&A*, 126, 7
 Bartel, N., & Bietenholz, M. F. 2003, *ApJ*, 591, 301
 —. 2008, *ApJ*, 682, 1065
 Bartel, N., Bietenholz, M. F., Rupen, M. P., & Dwarkadas, V. V. 2007, *ApJ*, 668, 924
 Bartel, N., Rupen, M. P., Shapiro, I. I., Preston, R. A., & Rius, A. 1991, *Nature*, 350, 212
 Bartel, N., et al. 1987, *ApJ*, 323, 505
 —. 2002, *ApJ*, 581, 404
 Beck, R., & Krause, M. 2005, *Astronomische Nachrichten*, 326, 414
 Bietenholz, M. F., & Bartel, N. 2008a, *Advances in Space Research*, 41, 424
 —. 2008b, *MNRAS*, 386, 1411
 Bietenholz, M. F., Bartel, N., & Rupen, M. P. 2000, *ApJ*, 532, 895
 —. 2001, *ApJ*, 557, 770
 —. 2002, *ApJ*, 581, 1132
 —. 2004a, *Science*, 304, 1947
 —. 2004b, *ApJ*, 615, 173
 —. 2005, *Advances in Space Research*, 35, 1052
 Bietenholz, M. F., Kassim, N., Frail, D. A., Perley, R. A., Erickson, W. C., & Hajian, A. R. 1997, *ApJ*, 490, 291
 Chandra, P., Ray, A., & Bhatnagar, S. 2004, *ApJ*, 612, 974
 Chevalier, R., & Blondin, J. M. 1995, *ApJ*, 444, 312
 Chevalier, R. A. 1982, *ApJ*, 259, 302
 —. 1987, *Nature*, 329, 611
 —. 1998, *ApJ*, 499, 810
 —. 2005, *ApJ*, 619, 839
 Chevalier, R. A., & Fransson, C. 1992, *ApJ*, 395, 540
 Chugai, N. N. 1993, *ApJ*, 414, L101
 Chugai, N. N., & Danziger, I. J. 1994, *MNRAS*, 268, 173
 Falcke, H., Körding, E., & Markoff, S. 2004, *A&A*, 414, 895
 Ferrarese, L., et al. 2000, *ApJS*, 128, 431
 Fey, A. L., et al. 2004, *AJ*, 127, 3587
 Fransson, C., & Björnsson, C.-I. 2005, in *IAU Colloq. 192: Cosmic Explosions, On the 10th Anniversary of SN1993J*, ed. J.-M. Marcaide & K. W. Weiler, 59
 Gaensler, B. M., & Slane, P. O. 2006, *ARA&A*, 44, 17
 Green, D. A. 2004, *Bulletin of the Astronomical Society of India*, 32, 335
 Gull, S. F. 1973, *MNRAS*, 161, 47
 Hales, A. S., et al. 2004, *ApJ*, 613, 977
 Ho, L. C. 2008, *ARA&A*, 46, 475
 Hobbs, G., Lorimer, D. R., Lyne, A. G., & Kramer, M. 2005, *MNRAS*, 360, 974
 Houck, J. C. 2005, in *X-Ray and Radio Connections* (eds. L.O. Sjouwerman and K.K Dyer) Published electronically by NRAO, <http://www.aoc.nrao.edu/events/xraydio> Held 3-6 February 2004 in Santa Fe, New Mexico, USA, (E3.03) 6 pages
 Houck, J. C., Bregman, J. N., Chevalier, R. A., & Tomisaka, K. 1998, *ApJ*, 493, 431
 Jones, T. W., et al. 1998, *PASP*, 110, 125
 Jun, B., & Norman, M. L. 1996, *ApJ*, 465, 800
 Kovalev, Y. Y., Lobanov, A. P., Pushkarev, A. B., & Zensus, J. A. 2008, *A&A*, 483, 759
 Kraan-Korteweg, R. C. 1986, *A&AS*, 66, 255
 Leibundgut, B., Kirshner, R. P., Pinto, P. A., Rupen, M. P., Smith, R. C., Gunn, J. E., & Schneider, D. P. 1991, *ApJ*, 372, 531
 Lundqvist, P., & Fransson, C. 1988, *A&A*, 192, 221
 Lyne, A. G., & Graham-Smith, F. 1990, *Pulsar astronomy*, ed. F. Lyne, A. G. & Graham-Smith
 Milisavljevic, D., Fesen, R. A., Leibundgut, B., & Kirshner, R. P. 2008, *ApJ*, 684, 1170
 Pacholczyk, A. G. 1970, *Radio astrophysics. Nonthermal processes in galactic and extragalactic sources* (San Francisco: Freeman)
 Pérez-Torres, M. A., Alberdi, A., Marcaide, J. M., Guirado, J. C., Lara, L., Mantovani, F., Ros, E., & Weiler, K. W. 2002, *MNRAS*, 335, L23
 Pradel, N., Charlot, P., & Lestrade, J.-F. 2006, *A&A*, 452, 1099
 Rupen, M. P., van Gorkom, J. H., Knapp, G. R., Gunn, J. E., & Schneider, D. P. 1987, *AJ*, 94, 61
 Smith, N., Hinkle, K. H., & Ryde, N. 2009, *AJ*, 137, 3558
 Smith, N., Humphreys, R. M., Davidson, K., Gehrz, R. D., Schuster, M. T., & Krautter, J. 2001, *AJ*, 121, 1111
 Tonry, J. L., Dressler, A., Blakeslee, J. P., Ajhar, E. A., Fletcher, A. B., Luppino, G. A., Metzger, M. R., & Moore, C. B. 2001, *ApJ*, 546, 681
 Tully, R. B. 1988, *Nearby galaxies catalog* (Cambridge and New York, Cambridge University Press, 1988, 221 p.)
 van Gorkom, J., Rupen, M., Knapp, G., Gunn, J., Neugebauer, G., & Matthews, K. 1986, *IAU Circ.*, 4248, 1
 Weiler, K. W., Panagia, N., Montes, M. J., & Sramek, R. A. 2002, *ARA&A*, 40, 387
 Weiler, K. W., Panagia, N., & Sramek, R. A. 1990, *ApJ*, 364, 611
 Weiler, K. W., Williams, C. L., Panagia, N., Stockdale, C. J., Kelley, M. T., Sramek, R. A., Van Dyk, S. D., & Marcaide, J. M. 2007, *ApJ*, 671, 1959